Liquid Crystals
Publication details, including instructions for authors and subscription information:
http://www.informaworld.com/smpp/title~content=t713926090

Switching and electrical properties of ferro- and antiferroelectric phases of MOPB(H)PBC

Anoop Kumar Srivastava[ab]; Ravindra Dhar[c]; Vinai Krishna Agrawal[a]; Seung Hee Leeb[b]; Roman Dabrowski[d]
[a] Physics Department, University of Allahabad, Allahabad-211 002, India [b] Polymer BIN Fusion Research Center, Department of Polymer Nano-Science and Technology, Chonbuk National University, Chonbuk 561-756, Korea [c] Physics Department, Ewing Christian College, Allahabad-211 003, India [d] Institute of Chemistry, Military University of Technology, Warsaw, Poland

To cite this Article Srivastava, Anoop Kumar , Dhar, Ravindra , Agrawal, Vinai Krishna , Leeb, Seung Hee and Dabrowski, Roman(2008) 'Switching and electrical properties of ferro- and antiferroelectric phases of MOPB(H)PBC', Liquid Crystals, 35: 9, 1101 — 1108
To link to this Article: DOI: 10.1080/02678290802389563
URL: http://dx.doi.org/10.1080/02678290802389563

Liquid Crystals,
Vol. 35, No. 9, September 2008, 1101–1108

Taylor & Francis
Taylor & Francis Group

Switching and electrical properties of ferro- and antiferroelectric phases of MOPB(H)PBC

Anoop Kumar Srivastava[a,b]*, Ravindra Dhar[a,c], Vinai Krishna Agrawal[a], Seung Hee Lee[b]* and Roman Dabrowski[d]

[a]*Physics Department, University of Allahabad, Allahabad-211 002, India;* [b]*Polymer BIN Fusion Research Center, Department of Polymer Nano-Science and Technology, Chonbuk National University, Chonju, Chonbuk 561-756, Korea;* [c]*Physics Department, Ewing Christian College, Allahabad-211 003, India;* [d]*Institute of Chemistry, Military University of Technology, 00-908, Warsaw, Poland*

(*Received 14 November 2007; final form 5 August 2008*)

Switching and dielectric relaxation phenomena were investigated for an antiferroelectric liquid crystal, 4,4-(1-methyloctyloxycarbonyl)phenyl]-4′-[3-(butanoyloxy)prop-1-oxy]biphenyl carboxylate, exhibiting chiral smectic A (SmA*), smectic C (SmC*) and antiferroelectric (SmC_A*) phases. Spontaneous polarisations, rotational viscosities, relaxation frequencies, dielectric strengths and distribution parameters were determined as a function of temperature. The electric field required for saturation of the spontaneous polarisation increased with a decrease in temperature. In the SmA* phase, only one relaxation mechanism was observed that behaves as soft mode. Two relaxation processes were detected in the SmC* phase. A high-frequency relaxation process invariant at 2.2 kHz was due to a Goldstone mode, but the origin of low-frequency relaxation process (1–20 Hz) is unclear; however, it may belong to an X-mode. The dielectric spectrum of the SmC_A* phase exhibits two absorption peaks separated by two decades of frequency. The low-frequency peak is related to the antiferroelectric Goldstone mode, whereas the high-frequency peak originates from the anti-phase fluctuation of the directors in the anti-tilt pairs of the SmC_A* phase.

Keywords: antiferroelectric liquid crystal; spontaneous polarisation; rotational viscosity; response time; dielectric relaxation; Goldstone mode; soft mode

1. Introduction

The first instance of anticlinic order, identified in a tilted chiral smectic phase during 1989–1990 (*1*), posed new challenges to understand interlayer structures, layer geometry in devices and electric-field induced switching mechanisms. Antiferroelectric liquid crystals (AFLCs) are attractive for use in devices owing to their tri-state switching behaviour, easy dc compensation, microsecond response, hemispherical viewing angle (in-plane switching geometry), grey scale capability and the absence of ghost effects (*2–7*). In most AFLCs, spontaneous polarisation usually decreases with increasing temperature and vanishes at the transition between chiral smectic C (SmC*) and smectic A (SmA*) phases (*8, 9*); spontaneous polarisation emerges perpendicular to the tilt plane (*10*), reflecting the polar properties of the liquid crystal.

Dielectric spectroscopy is one of the most important tools used to study the collective and molecular dynamics of different phases lying between the isotropic and the crystalline phases. For example, a collective process in a paraelectric SmA* phase is detected in the dielectric permittivity, $\varepsilon'_{\perp}$, which has a contribution from director tilt fluctuations (soft mode) (*11–13*). In the ferroelectric SmC* phase, the $\varepsilon'_{\perp}$, besides the soft mode, reveals another collective mode due to phase fluctuations (Goldstone mode) (*11–13*). In addition to Goldstone and soft modes, dielectric measurements have shown the existence of other relaxation modes in surface-stabilised FLC cells or under a biased electric field (*14–17*). The dielectric spectrum of an antiferroelectric (SmC_A*) phase contains two characteristic relaxation modes (P_L, P_H) observed in the kHz and MHz regions, respectively (*18–27*). In some investigations, the P_L process has been interpreted as non-collective molecular reorientation around the short axis (18–20]), a process that is usually observed in the quasi-homeotropic orientation of tilted smectics. However, other researchers have interpreted this process as a helical Goldstone mode due to coupling between the existence of small residual polarisation in antiferroelectric phase and applied electric field, $\delta P.E$ (*26, 27*). This mode was attributed to in-phase azimuthal angle fluctuations by Buivydas *et al.* (*25*). Furthermore, Panarin *et al.* (*26, 27*) reported that the P_L mode may be due to distortion of an antiferroelectric helix because of coupling between dielectric anisotropy and electric field, $\Delta\varepsilon.E^2$. However, this process can not be detected during dielectric measurements. The origin of the P_H process is known to be associated with anti-phase azimuthal

*Corresponding authors. Emails: srivastava_anoop@rediffmail.com (A.K. Srivastava); Lsh1@chonbuk.ac.kr (S.H. Lee)

ISSN 0267-8292 print/ISSN 1366-5855 online

DOI: 10.1080/02678290802389563
http://www.informaworld.com

angle fluctuations of the director of anti-tilt molecules in successive layers (*25–27*). In the MHz region, almost all the liquid crystalline phases exhibit two high-frequency molecular processes corresponding to the molecular rotation of the molecules around their long and short axes (*27, 28*).

In this paper, spontaneous switching and detailed dielectric spectroscopy are reported for a novel AFLC, 4,4-(1-methyloctyloxycarbonyl)phenyl]-4′-[3-(butanoyloxy)prop-1-oxy]biphenyl carboxylate [MOPB(H)PBC], which has the chemical structure shown in Scheme 1. MOPB(H)PBC exhibits both ferroelectric (SmC*) and antiferroelectric (SmC_A*) phases.

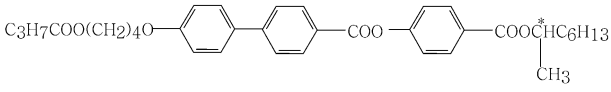

Scheme 1. Chemical structure of MOPB(H)PBC.

2. Experimental

Different mesophase transition temperatures were determined using differential scanning calorimetry (DSC) and polarising optical microscopy (POM). Spontaneous polarisation (P_s) and rotational viscosity (γ) were measured (*29, 30*) in a planar aligned cell, with the help of automatic liquid crystal tester (ALCT), by applying a triangular wave electric field of $21\,V\,\mu m^{-1}$ with a frequency of 8 Hz across a cell with an active area (A) of $0.25\,cm^2$ and electrode spacing (d) of 4.7 μm. The ALCT uses the traditional field reversal technique (*29, 30*) to determine the spontaneous polarisation. In FLC/AFLC phases, for a certain applied voltage, V, the current response, I, consists of three components: the capacitive term (I_C), the ionic conduction term (I_R) and the polarisation current (I_P) due to the charge induced by the dipole realignment in the form of polarisation hump. The area under the hump is a measure of the spontaneous polarisation (P_s), which is given by

$$P_s = \frac{A(V \times t)}{R(\text{Area of the sample})}, \qquad (1)$$

where $A(V \times t)$ is the area under the curve in terms of voltage (V) and time (t) and $R = 500\,k\Omega$ is the standard resistance internally connected in the ALCT. The ALCT directly gives the results of spontaneous polarisation by selecting the observed polarisation hump on applied electric field. In addition, ALCT measurements were also used to determine the rotational viscosity (γ) by using (*31*)

$$\gamma = \frac{AP_s^2 V_m}{I_m d}, \qquad (2)$$

where I_m is the peak value of the polarisation current observed at voltage V_m.

Dielectric studies of the planar and homeotropically aligned samples were carried out in the frequency range from 0.1 Hz to 10 MHz by using an impedance gain phase analyser (Solartron model SI-1260) coupled with a dielectric interface (Solartron model SI-1296). For the dielectric measurements, low-resistance (~25 Ω/sheet) ITO-coated glass electrodes were used. Two electrodes (coated with nylon and then rubbed unidirectionally) of the dielectric cell were separated by mylar spacers of thickness 10 μm. The active capacitance of the dielectric cell was determined by using standard liquid cyclohexane and it was cross-checked by a geometrical method. The temperature of the sample was controlled with the help of a hot stage (Instec model HS-1) with an accuracy of 0.1°C. A measuring electric field of $0.5\,V_{rms}$ was applied across the sample through the electrodes.

3. Results and discussion

Peak transition temperatures of MOPB(H)PBC were determined by DSC at different scanning rates ranging between 1.0 and 15.0°C min^{-1}. Figure 1 shows the DSC thermogram on cooling at a rate of 2.5°C min^{-1}.

It was observed that peak transition temperatures (T_p) vary linearly with the scanning rate. Using a least squares fit of T_p with scanning rate (in °C min^{-1}), extrapolated transition temperatures at a scanning rate of 0°C min^{-1} were determined and taken as true transition temperatures (*32*). MOPB(H)PBC was found to exhibit the following phase sequence on cooling (extrapolated transition temperatures at a scan rate of 0°C min^{-1}):

I 108.7°C SmA* 98.1°C SmC* 88.2°C SmC_A* 51.9°C Cr.

Different phases were identified by using POM.

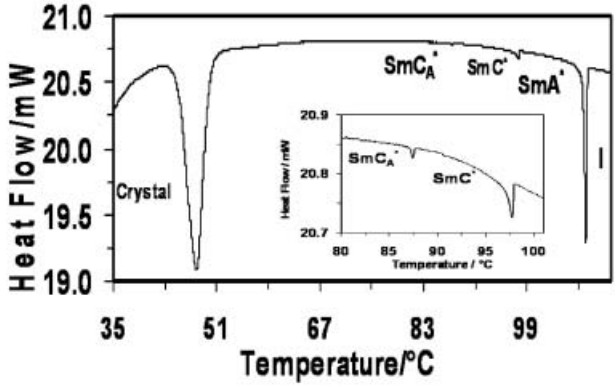

Figure 1. DSC thermogram of MOPB(H)PBC on cooling cycle at a rate of 2.5°C min^{-1}.

Polarisation switching responses

When elastic constants are ignored, the director motion of the FLC molecules can be described as (*15*)

$$\gamma \frac{\partial \phi}{\partial t} = -P_s E \sin\phi, \tag{3}$$

where ϕ is the angle between dipole and the cell normal and E is the applied electric field.

Solution of Equation (3) gives the response time for switching the sample

$$\tau_r = \gamma / P_s E. \tag{4}$$

τ_r is the delayed switching time between two stable states of polarisation (*33*). In general, a large P_s and low γ are needed for quick electro-optical response. The switching time was estimated by using Equation (4). The temperature dependences of the polarisation switching parameters, P_s, γ and τ_r, are shown in Figure 2. No anomaly was detected in the P_s and γ curves at the SmC*–SmC$_A$* phase transition. The continuous line fits the power law

$$P_s = P_0 \left(1 - \frac{T}{T_C}\right)^{\beta}. \tag{5}$$

The value of P_0 obtained from fittings is 250.1 nC cm^{-2}, whereas the estimated value of β was found to be 0.32, which was smaller than theoretical value of β=0.5 predicted for a second-order transition (*34*). The estimated response time was found to be less than 11 µs over the whole temperature range used in this study.

The electric field-dependent spontaneous polarisation at different temperatures has also been measured (Figure 3). It is apparent from Figure 3 that a high electric field is required to obtain saturation of P_s with a decrease in temperature. At 82°C, the P_s saturates at an applied voltage of ~40 V, whereas at 62°C the voltage required for saturation of P_s goes up to ~90 V.

Dielectric relaxations

To analyse the measured dielectric data, the dielectric spectrum was fitted using the generalised Cole–Cole Equation:

$$\varepsilon^* = \varepsilon' - j\varepsilon'' = \varepsilon(\infty) + \sum_{i=1}^{2} \frac{(\Delta\varepsilon)_i}{1 + \left(j\frac{f}{f_{ri}}\right)^{(1-h_i)}} + \frac{A_1}{f^n} - j\frac{\sigma_i}{2\pi\varepsilon_0 f^k} - jA_2 f^m \tag{6}$$

where $\varepsilon(\infty)$ is the relative permittivity in the high-frequency limit and $\Delta\varepsilon_i$, f_{ri} and h_i are the dielectric strength, relaxation frequency and distribution parameter ($0 \leqslant h_i \leqslant 1$), respectively, of the i^{th} mode. The

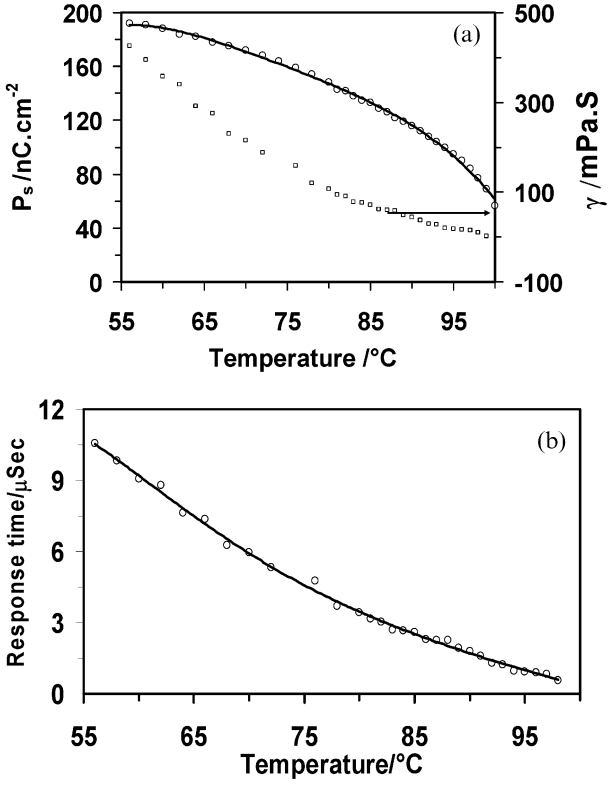

Figure 2. (a)Variation of the spontaneous polarisation (P_s) and rotational viscosity (γ)of MOPB(H)PBC with temperature. (b) Variation of response time (τ) with temperature.

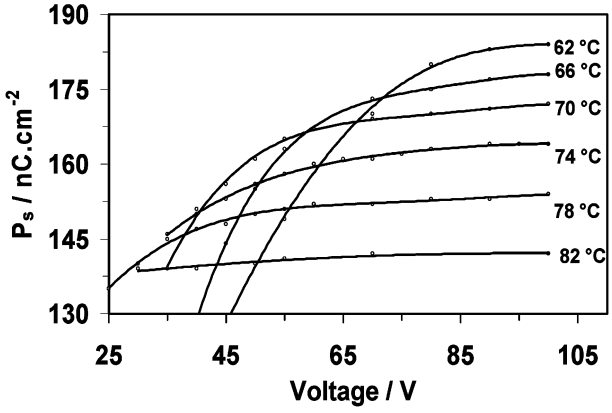

Figure 3. Variation of spontaneous polarisation (P_s) of MOPB(H)PBC with applied voltage (V) at different temperatures.

third term of Equation (6) represents the contribution of electrode polarisation capacitance at low frequencies (*35*), where A_1 and n are fitting parameters. $\frac{\sigma_i}{2\pi\varepsilon_0 f^k}$ accounts for the contribution of ionic conductivity, with σ_i and k as fitting parameters (usually $k=1$). ε_0 ($=8.85\,\mathrm{pF\,m^{-1}}$) is the permittivity of free space. The measured dielectric absorption, $\varepsilon''_\perp$, contains a contribution above 100 kHz due to the finite resistance of ITO-coated electrodes (*36*). An additional imaginary term (*37*), $A_2 f^m$, is empirically added in Equation (6) to partially account for this effect, where A_2 and m are fitting constants.

Different parameters were estimated by fitting the experimental curve of real $(\varepsilon'_\perp)$ and imaginary $(\varepsilon''_\perp)$ parts of Equation (6) at different frequencies in the temperature interval from 103.0°C to 58.0°C. Variation of the dielectric strength ($\Delta\varepsilon$) and relaxation frequency (f_r) of different modes with temperature is shown in Figures 4 and 5, respectively.

The relaxation mode observed in the SmA* phase was identified as a soft mode on the basis of the temperature dependence of $\Delta\varepsilon$ and f_r. The soft mode dielectric strength ($\Delta\varepsilon_s$) and relaxation frequency (f_s) in the SmA* phase vary strongly with temperature. $\Delta\varepsilon_s^{-1}$ is observed to increase linearly with temperature, as shown in Figure 6.

The values of $\Delta\varepsilon_s$ were fitted (*12*) to the following Equation in the temperature range 100.1–103.0°C:

$$\varepsilon_0\Delta\varepsilon_s = \frac{\varepsilon_0^2\varepsilon^2(\infty)C^2/\alpha T_C}{\left(\frac{T}{T_C}-1\right)^{\gamma_1} + Kq_0^2/\alpha T_C} \qquad (7)$$

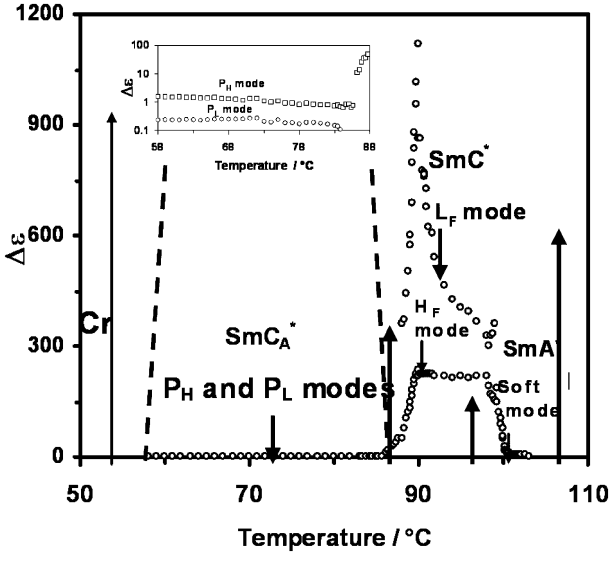

Figure 4. Temperature dependence of the dielectric strengths ($\Delta\varepsilon$) of various relaxation modes in SmA*, SmC* and SmC_A* phases of MOPB(H)PBC. Vertical arrows show the transition temperature as obtained by DSC.

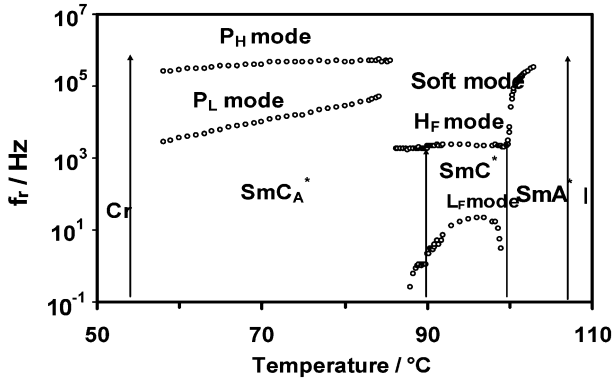

Figure 5. Temperature dependence of relaxation frequencies (f_r) in SmA*, SmC* and SmC_A* phases of MOPB(H)PBC. Vertical arrows show the transition temperature observed by DSC.

where T_C is Curie (paraelectric to ferroelectric transition) temperature, $q_0=2\pi/\text{pitch}$ and $\frac{\varepsilon_0\varepsilon^2(\infty)C^2}{\alpha}$ is a term arising owing to the coupling between tilt and polarisation. Kq_0^2/α $\left(K=K_{33}-\varepsilon_0\varepsilon(\infty)\mu^2\right)$ is the temperature-equivalent energy needed to unwind the helical structure at the SmC*–SmA* transition. C and μ are the coefficients of flexo- and piezoelectric coupling between director gradient and polarisation, and between tilt and polarisation, respectively. K_{33} is the bend elastic constant and γ_1 is a critical exponent, which has been incorporated to account for the deviation from the linearity in $1/\varepsilon_S$, if any. Assuming that $\varepsilon(\infty)$, C, α, q_0 and K are not sensitive to temperature in the range 100.1–103.0°C, evaluated values of fitting parameters are listed in Table 1. From the fitting, γ_1 is found to be 1, which shows that material is the following Curie–Weiss law. The cut-off value of dielectric strength is given by the ratio

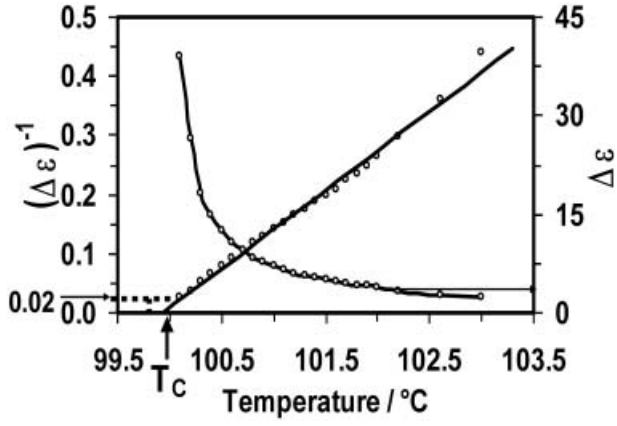

Figure 6. Variation of dielectric strength ($\Delta\varepsilon$) of MOPB(H)PBC and its inverse ($\Delta\varepsilon^{-1}$) with temperature for soft mode in the SmA* phase.

Table 1. Values of fitting parameters according to equation (7).

$\frac{\varepsilon_0\varepsilon^2(\infty)C^2}{\alpha}$ (K)	$\frac{Kq_0^2}{\alpha}$ (K)	$\frac{\varepsilon_0\varepsilon^2(\infty)C^2}{Kq_0^2}$	T_C (°C)	γ_1
6.74±0.17	0.1418±0.0004	47.7	100.1	1

$\frac{\varepsilon_0\varepsilon^2(\infty)C^2}{Kq_0^2}$, which is 47.5. Experimentally, the value of dielectric strength at 100.1°C is found to be 48.8, i.e. at T_C, $1/\Delta\varepsilon=0.02$ (see Figure 6).

In contrast to the dielectric strength and relaxation frequency of the soft mode in SmA* phase, the dielectric strength (~215) and relaxation frequency (~2.2 kHz) for the high-frequency relaxation mode (H_F) of the SmC* phase are almost independent of the temperature (see Figures 4–5). Hence, it has been identified as the Goldstone mode. The dielectric strength of this mode increases rapidly just below T_C (=100.1°C) and exhibits a maximum at 98.0°C. Usually this maximum in the dielectric response is connected with the maximum exhibited by the helical pitch (*37*). Another mode (L_F), in the low-frequency region, has also been observed in the SmC* phase. The relaxation frequency of L_F mode initially increases from 3 Hz at 99°C to 21 Hz at 96°C; however, with further decrease in temperature, the relaxation frequency of this mode starts to decrease. The dielectric strength of the L_F mode increases from ~330 at 99°C to ~670 at 91°C. The L_F mode has some similarity with the behaviour of soft mode as its relaxation frequency increases near the transition temperature T_C. Relaxation frequencies and dielectric strengths are also strongly temperature dependent. But it can not be the soft mode, because, below T_C, the dielectric strength of the L_F mode increases with decrease in temperature. Also this mode may not be due space charge accumulation on the interfaces between liquid crystal and polyamide nylon coating because space charge accumulation on the interfaces between liquid crystal and polyamide nylon coating have been taken care by the terms $A_1 f^{-n}$ in ε' and $\sigma/2\pi\varepsilon_0 f$ in ε'' in Equation (6) and, moreover, this mode was observed only in the SmC* phase. Beresnev *et al.* (*14*) have also reported two modes in the SmC* phase that were connected to the domain modes (D_B and D_S modes), but these modes could only be observed after suppression of Goldstone mode with biased electric field. The L_F mode may belong to an X-mode caused by distortion of pretilt angle because an X-mode may appear even in absence of bias electric field (*15–17*). Furthermore, temperature dependent variations of dielectric strength and relaxation frequency of L_F mode are the same as those reported by Wang *et al.* (*16*).

The dielectric spectrum of the SmC_A* phase exhibited two absorption peaks P_L and P_H separated by at least two decades of frequency, as shown in Figure 7. Thermodynamically, it was observed that the SmC*–SmC_A* transition temperature is 88.2°C. From dielectric measurements, the transition to the SmC_A* phase starts at 90.0°C and completes at 86.2°C. In this temperature range, pre-transitional effects are manifested such that the relaxation frequency remains constant (~1.8 kHz) with temperature, and the dielectric strength decreases with decrease in temperature, as shown in Figure 8. It seems that in this temperature interval there is a competition between the structures of SmC* and SmC_A*, prior to transformation of the material to SmC_A*. The P_H antiferroelectric mode appeared at 85.6°C; however, the P_L mode was visible at around 84.2°C. The relaxation frequencies of both the modes

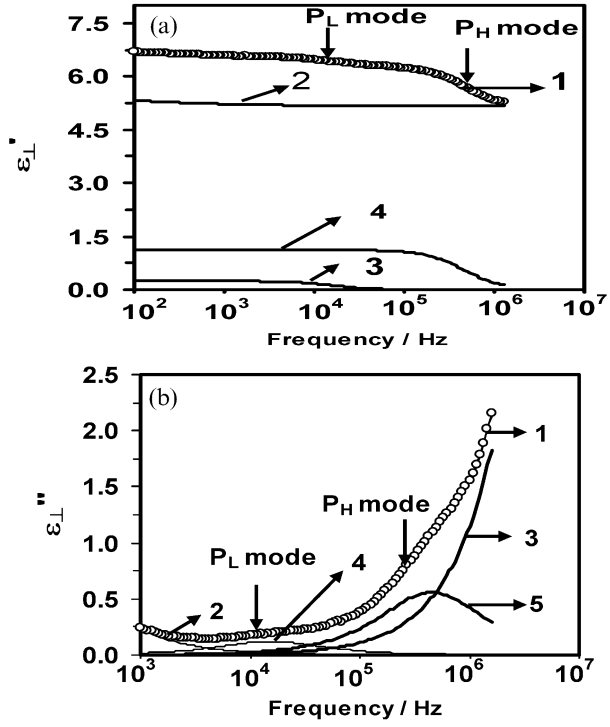

Figure 7. (a) Variation of dielectric permittivity $(\varepsilon'_\perp)$ (a) and loss $(\varepsilon''_\perp)$ (b) with frequency at 75.0°C in the SmC_A* phase of MOPB(H)PBC. Circles of curve 1 show the experimental data, whereas the continuous line on circles shows best fitting according to equation (6). In (a), curve 2 represents the low-frequency correction term along with the $\varepsilon(\infty)$; curve 3 (P_L mode) and curve 4 (P_H mode) have been resolved after subtracting the low-frequency correction terms. In (b), curves 2 and 3 represent the low- and high-frequency correction terms; curves 4 (P_L mode) and 5 (P_H mode) have been resolved after subtracting the low- and high-frequency correction terms.

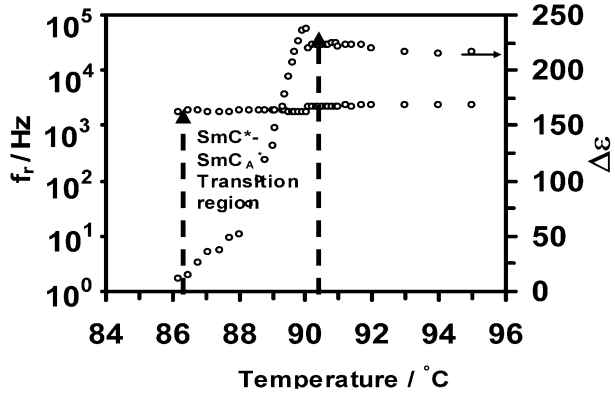

Figure 8. Temperature dependence of dielectric strength ($\Delta\varepsilon$) and relaxation frequency (f_r) of MOPB(H)PBC in the temperature range 86.0–96.0°C. In the SmC*–SmC$_A$* transition region the relaxation frequency is constant, whereas the dielectric strength decreases with decrease in temperature, as shown between the vertical dotted lines.

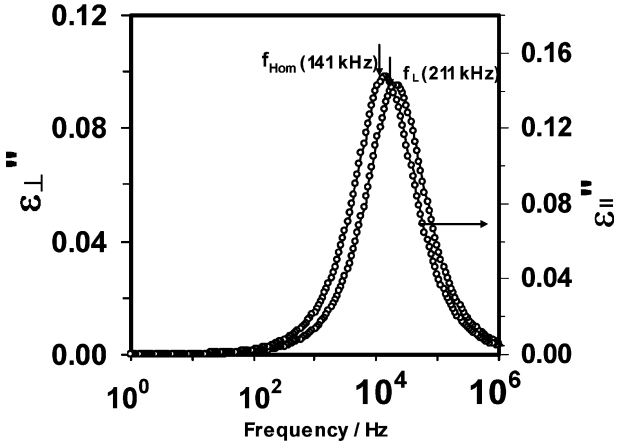

Figure 9. Variation of dielectric loss of MOPB(H)PBC at 77.0°C for planar and homeotropically aligned molecules/ sample.

decrease almost linearly with temperature. However, the dielectric strengths are weakly temperature dependent. The temperature dependent relaxation frequency of the both the modes can be fitted to the Arrhenius law:

$$f = f_0 \exp(E_a/k_B T), \tag{8}$$

where f_0 is constant parameter, k_B ($=1.38\times 10^{-23}\,\mathrm{J\,K^{-1}}$) is the Boltzman constant, E_a is an activation energy and T is the temperature in K. P_L and P_H modes have activation energies of 1.06 eV, and 0.30 eV respectively.

Buivydas *et al.* (*21*) have reported that the P_L process cannot be connected with molecular reorientation around the short axis, because the relaxation frequency of this process should be same at particular temperature for both planar and homeotropically aligned samples. To verify this, a dielectric experiment on a homeotropic cell was also performed. A single relaxation phenomenon was observed over the whole temperature range. Dielectric absorptions of planar and homeotropically aligned samples at 77.0°C are shown in Figure 9. The relaxation frequency for homeotropic aligned sample is less than that of planar aligned sample at this temperature, and hence the P_L process can not be connected with molecular reorientation around the short axis.

The low-frequency mode (P_L) of the SmC$_A$* phase has features typical of a Goldstone mode. It is well known that a helicoidal superstructure exists in the SmC$_A$* phase, with anti-tilt pair spiralling in a specific direction. The *c*-directors in the adjacent smectic layers of the SmC$_A$* phase are not completely anti-parallel to each other, so that there is a slight imbalance in the local polarisation. This causes 'antiferroelectric spontaneous polarisation', δP. Such 'antiferroelectric polarisation' will spiral about the helical axis, as does polarisation in the ferroelectric (SmC*) phase (*26, 27*). Hence, we can expect the dielectric relaxation process to arise from the distortion of the antiferroelectric helix, similar to that of the ferroelectric Goldstone mode, although with a low dielectric strength, as also observed by Panarin *et al.* (*26, 27*). The high-frequency mode (P_H) is believed to originate from fluctuations of the directors in the anti-tilt pairs of the SmC$_A$* phase, where they rotate in opposite phase; hence, it is called the anti-phase azimuthal angle fluctuation mode (*25–27*). In the present work, the dielectric strengths of P_L mode ($\Delta\varepsilon_{P_L\ \mathrm{mode}} = \sim 0.07 - 0.24$) were found to be smaller than that of the P_H mode ($\Delta\varepsilon_{P_H\ \mathrm{mode}} = \sim 0.77 - 1.62$). On the basis of the dielectric strengths, we have given the same assignments to P_L and P_H of the present work as those suggested by Panarin *et al.* (*27*).

Variation of the relaxation frequency in a homeotropically aligned cell is shown in Figure 10. As can be seen, the relaxation frequency decreases with decrease in temperature. Dielectric strength (not shown in figure) in a homeotropically aligned cell was nearly constant (~0.4) over the whole temperature range studied. Therefore, the relaxation process observed in the homeotropically aligned cell can be assigned due to the rotational fluctuation of the molecules about their short axes. The activation energy, of this mode was found to be 0.99 eV.

Variations of distribution parameters with temperatures for different modes are shown in Figure 11. The value of distribution parameter for Goldstone

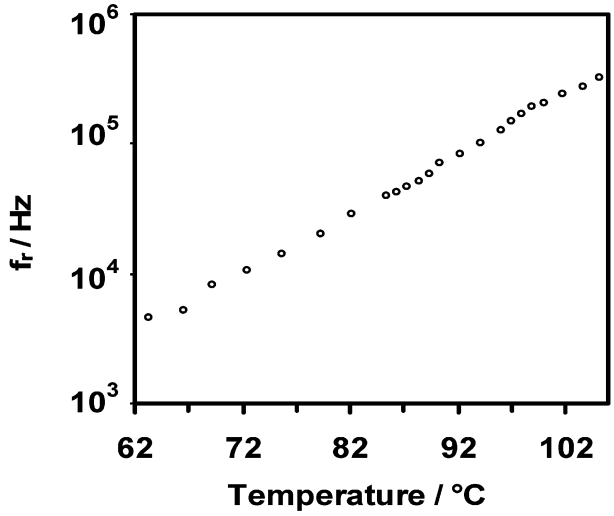

Figure 10. Temperature dependence of the relaxation frequency of MOPB(H)PBC for homeotropically aligned molecules.

mode is ~0.12 and increases near the SmA*–SmC* and SmC*–SmC_A* phase transition temperatures. The distribution parameter for the soft mode in the SmA* phase is ~0 and hence exhibits Debye-type relaxation process. For P_L and P_H modes, the estimated distribution parameter is ~0 and therefore these two modes also follow the Debye-type relaxation process.

Ionic conductivity

The ionic conductivity has been determined in different mesophases by fitting the fourth term of Equation (6) to the dielectric spectra. In different mesophases, it has been observed that ionic conductivity decreases with decrease in temperature and it follows an Arrhenius behaviour. Values of ionic conductivity estimated from Equation (6) in different mesophases are of the order of 10^{-7}–10^{-9} S m^{-1}. The value of ionic conductivity in the SmA* phase is of the order of 10^{-7} S m^{-1}, whereas in the SmC* phase it is of the order of 10^{-7}–10^{-8} S m^{-1}. For the SmC_A* phase (including pre-transitional effect), the value of ionic conductivity is of the order of 10^{-8}–10^{-9} S m^{-1}. The activation energy of ionic conductivity has been derived in different phases using the following relation:

$$\sigma = \sigma_0 \exp\left(-\frac{E_a}{k_B T}\right), \tag{9}$$

where σ_0 is a constant. Variation of ln(σ) with the inverse of absolute temperature ($1/T$) is shown in Figure 12. Discontinuities are observed at the SmA*–SmC*, SmC*-pretransitional effects and pretransitional effects-SmC_A* phases. The activation energy for ionic conductance of different mesophases has been determined with the help of a least squares fit method. The value of the activation energy in the SmA* phase is found to be 0.29 eV, whereas in the SmC* and SmC_A* (excluding pre-transitional effect) phases the values of the activation energies were 0.86 eV and 0.73 eV, respectively. It is interesting to note that activation energy of ionic conductivity in SmA* phase is smaller than those of SmC* and SmC_A* phases. This shows that the probability of collisions of ions with liquid crystal molecules in SmC* and SmC_A* phases is larger than that of the SmA* phase.

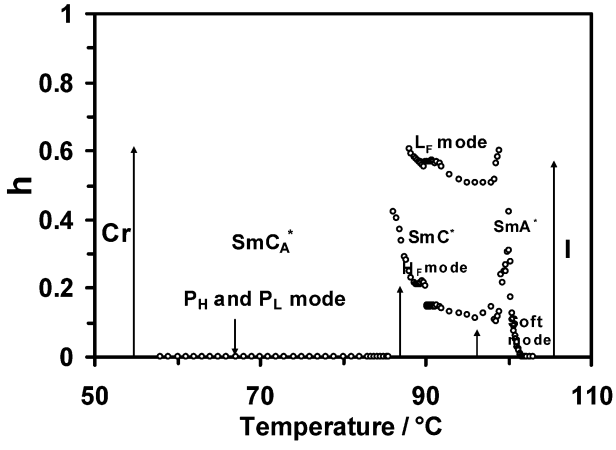

Figure 11. Variation of distribution parameter with temperature in the SmA*, SmC* and SmC_A* phases of MOPB(H)PBC. Vertical arrows show the transition temperatures observed by DSC.

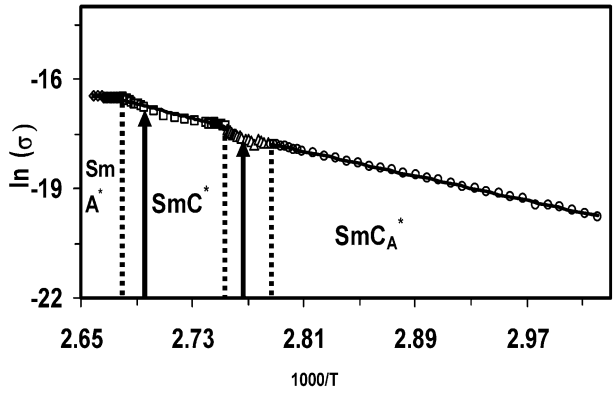

Figure 12. Temperature dependence of ln(σ) in the SmA*, SmC* and SmC_A* phases of MOPB(H)PBC. Rhombuses represent the SmA* phase, squares the SmC* phase, triangles the pre-transitional effects and circles the SmC_A* phase. Vertical arrows show the transition temperatures observed by DSC, whereas dashed lines show the phase transition temperatures observed by dielectric measurements.

4. Conclusions

The polarisation switching and electrical properties of AFLC material MOPB(H)PBC have been investigated. The material possesses moderate spontaneous polarisation (~100–200 nC cm^{-2}) and microsecond response time (1–10 μs). Spontaneous polarisation, rotational viscosity and response time were found to increase with decrease in temperature. Dielectric spectroscopy of the material reveals one relaxation process in the paraelectric (SmA*) phase, which is related to the soft mode. The soft mode in the SmA* phase follows the Curie–Weiss law, with a Currie temperature T_C=100.1°C. Two relaxation processes have been detected in the ferroelectric (SmC*) phase, in which a high-frequency relaxation (H_F mode) is related to the Goldstone mode, whereas the origin low-frequency relaxation process (L_F mode) may belong to an X-mode. The dielectric spectroscopic analysis revealed co-existence of SmC* and SmC_A* phases spread over a temperature interval of ~5°C. Two relaxation modes observed in the SmC_A* phase are due to the collective phase fluctuation (Goldstone mode) associated with helicoidal superstructure (P_L mode) and collective rotation of directors in two adjacent smectic layers in the opposite sense (P_H mode). Higher values of activation energy for ionic conductance in SmC* and SmC_A* phases (~0.8 eV) as compared to SmA* (~0.3 eV) shows that probability of collisions of ions with liquid crystal molecules in SmC* and SmC_A* phases is larger than that of the SmA* phase.

References

(1) Chandani A.D.L.; Hagiwarra T.; Suzuki Y.; Ouchi Y.; Takezoe H.; Fukuda A. *Jap. J. Appl. Phys.* **1988**, *27*, L729–L732; Chandani, A.D.L.; Ouchi, Y.; Takezoe, H.; Fukuda, A.; Terashima, K.; Furukawa, K.; Kishi. A. *Jap. J. Appl. Phys*. **1989,** *28,* L1261–L1264; Chandani, A.D.L.; Gorecka, E.; Ouchi, Y.; Takezoe, H.; Fukuda, A. *Jap. J. Appl. Phys.* **1989,** *28,* L1265–L1268.

(2) Castillo P.L.; Otón J.; Dabrowski R.; Lara A.; Quintana X.; Bennis N. *Proc. Int. Soc. Opt. Engng (SPIE)* **2004**, *5565*, 284–289.

(3) Quintana X.; Castillo P.L.; Otón J.; Bennis N.; Lara A.; Dabrowski R. *Proc. Int. Soc. Opt. Engng (SPIE)* **2004**, *5565*, 290–296.

(4) Dabrowski R.; Czuprynski K.; Gasowska J.; Oton J.; Quintana X.; Castillo P.L.; Bennis N. *Proc. Int. Soc. Opt. Engng (SPIE)* **2004**, *5565*, 66–71.

(5) Lagerwall S.T. *Ferroelectric and Antiferroelectric Liquid Crystals*; Wiley-VCH: Weinheim, 1999.

(6) Rudquist P.; Lagerwall J.P.F.; Meier J.G.; D'havé K.; Lagerwall S.T. *Phys. Rev. E* **2002**, *66*, 061708.

(7) Lagerwall S.; Dahlgren A.; Jagemalm P.; Rudquist P.; D'have K.; Pauwels H.; Dabrowski R.; Drzewinski W. *Adv. Funct. Mater.* **2001**, *11*, 87–84.

(8) Bilnc R. *Ferroelectrics* **1976**, *14*, 603–606.

(9) Srivastava A.K.; Agrawal V.K.; Dabrowski R.; Otón J.M.; Dhar R. *J. Appl. Phys.* **2005**, *98*, 013543.

(10) Miyachi K.; Matsushima J.; Takanishi Y.; Ishikawa K.; Takezoe H.; Fakuda A. *Phys. Rev. E* **1995**, *52*, R2153–R2156.

(11) Lesvstic A.; Carlsson T.; Filipic C.; Levstik I.; Zeks B. *Phys. Rev. A* **1987**, *35*, 3527–3584.

(12) Carlsson T.; Zeks B.; Filipic C.; Levstik I. *Phys. Rev. A* **1990**, *42*, 877–889.

(13) Gouda F.; Skarp K.; Lagerwall S.T. *Ferroelectrics* **1991**, *113*, 165–206.

(14) Beresnev L.; Pfeiffer M.; Pikin S.; Haase W.; Blinoov L. *Ferroelectrics* **1992**, *132*, 99–114.

(15) Panarin Y.P.; Xu H.; MacLughadha S.T.; Vij J.K. *Jap. J. Appl. Phys.* **1994**, *33*, 2648–2650.

(16) Wang J.M.; Kim J.J. *Jap. J. Appl. Phys.* **2000**, *39*, 5939–5942.

(17) Kundu S.K.; Yagihara S. *Jap. J. Appl. Phys.* **2007**, *46*, 3211–3213.

(18) Hiraoka K.; Taguchi A.; Ouchi Y.; Takezoe H.; Fukuda A. *Jap. J. Appl. Phys.* **1990**, *29*, L103–L106.

(19) Hatano J.; Hanakai Y.; Furue H.; Uehara H.; Satio S.; Murashiro K. *Jap. J. Appl. Phys.* **1994**, *33*, 5498–5502.

(20) Uehara H.; Hanakai Y.; Hatano J.; Satio S.; Murashiro K. *Jap. J. Appl. Phys.* **1995**, *34*, 5424–5428.

(21) Buivydas M.; Gouda F.; Andersson G.; Lagerwall S.T.; Stebler B.; Bomelburg J.; Heppke G.; Gestblom B. *Liq. Cryst.* **1997**, *23*, 723–739.

(22) Merino S.; de la Fuente M.R.; Gonzalez Y.; Perez Jubindo M.A.; Ros B.; Puertolas J.A. *Phys. Rev. E* **1996**, *54*, 5169–5177.

(23) Hou J.; Schacht J.; Giesselmann F.; Zugenmaier P. *Liq. Cryst.* **1997**, *22*, 409–417.

(24) Marzec M.; Mikulko A.; Wrobel S.; Haase W.; Dabrowski R. *Mol. Cryst. Liq. Cryst.* **2005**, *437*, 1413–1424.

(25) Buivydas M.; Gouda F.; Lagerwall S.T.; Stebler B. *Liq. Cryst.* **1995**, *18*, 879–886.

(26) Panarin Y.P.; Kalinvoskaya O.; Vij J.K. *Appl. Phys. Lett.* **1998**, *72*, 1667–1669.

(27) Panarin Y.P.; Kalinovskaya O.; Vij J.K. *Liq. Cryst.* **1998**, *25*, 241–252.

(28) Merino S.; de Daran F.; de la Fuente M.R.; Jubindo M.A.P.; Siera T. *Liq. Cryst.* **1997**, *23*, 275–283.

(29) Raina K.K.; Ahuja J.K. *Mol. Cryst. Liq. Cryst.* **1999**, *338*, 125–140.

(30) Srivastava S.L.; Agrawal V.K.; Beresnev L.A. *Indian J. Pure Appl. Phys.* **1993**, *31*, 30–35.

(31) ALCT Internal guide, Version 3.1 (unpublished), Instec, Inc, 5589 Arapahoe Ave., 208, Boulder, CO 80303, USA, Web: http://www.instec.com.

(32) Srivastava S.L.; Dhar R.; Kurik M.V. *Mol. Mater.* **1993**, *2*, 261–273.

(33) Ahuja J.K.; Raina K.K. *Jap. J. Appl. Phys.* **2000**, *39*, 4076–4081.

(34) Mikulko A.; Marzec M.; Wrobel S.; Dabrowski R. *Opto-Electron. Rev.* **2006**, *14*, 319–322.

(35) Srivastava S.L.; Dhar R. *Indian J. Pure Appl. Phys.* **1991**, *29*, 745–751.

(36) Srivastava S.L. *Proc. Natn. Acad. Sci. India.* **1993**, *63*, 311–332.

(37) Gouda F., Dielectric Relaxation Spectroscopy of Chiral Smectic Liquid Crystals. Ph.D. Thesis, Chalmers University of Technology, Gothenburg, 1992.